

Detectability of continuous gravitational waves from isolated neutron stars in the Milky Way: the population synthesis approach

Marek Cieřlar^{1,*}, Tomasz Bulik^{2,**}, Małgorzata Curyło², Magdalena Sieniawska^{2,1}, Neha Singh², and Michał Bejger¹

¹ Nicolaus Copernicus Astronomical Center, Polish Academy of Sciences, Bartycka 18, 00-716 Warsaw, Poland

² Astronomical Observatory, University of Warsaw, Al. Ujazdowskie 4, 00-478 Warsaw, Poland

February 18, 2021

ABSTRACT

Aims. We estimate the number of pulsars, detectable as continuous gravitational wave sources with the current and future gravitational-wave detectors, assuming a simple phenomenological model of evolving non-axisymmetry of the rotating neutron star.

Methods. We employ a numerical model of the Galactic neutron star population, with the properties established by comparison with radio observations of isolated Galactic pulsars. We generate an arbitrarily large synthetic population of neutron stars and evolve their period, magnetic field, and position in space. We use a gravitational wave emission model based on exponentially decaying ellipticity – a non-axisymmetry of the star, with no assumption of the origin of a given ellipticity. We calculate the expected signal in a given detector for a 1 year observations and assume a detection criterion of the signal-to-noise ratio of 11.4 – comparable to a targeted continuous wave search. We analyze the population detectable separately in each detector: Advanced LIGO, Advanced Virgo, and the planned Einstein Telescope. In the calculation of the expected signal we neglect signals frequency change due to the source spindown and the Earth motion with respect to the Solar barycentre.

Results. With conservative values for the neutron stars evolution: supernova rate once per 100 years, initial ellipticity $\epsilon_0 \approx 10^{-5}$ with no decay of the ellipticity $\eta = t_{\text{hub}} \approx 10^4$ Myr, the expected number of detected neutron stars is below one: 0.15 (based on a simulation of 10 M stars) for the Advanced LIGO detector. A broader study of the parameter space (ϵ_0, η) is presented. With the planned sensitivity for the Einstein Telescope, and assuming the same ellipticity model, the expected detection number is: 26.4 pulsars during a 1-year long observing run.

Key words. Stars: neutron – Gravitational waves – Methods: numerical

1. Introduction

The discovery of a double black hole merger (Abbott et al. 2016) and a binary neutron star (NS) merger (Abbott et al. 2017; Abbott et al. 2017) initiated an era of observable gravitational waves (GW) sources. The first catalogue of transient GW events (Abbott et al. 2019), created after two observational runs O1 and O2, contains 11 sources and the observational run O3 brought nearly 1 statistically-significant detection candidate per week¹ (Abbott et al. 2020). Still, some sources of the gravitational radiation, in particular the continuous waves from rotating, deformed (non-axisymmetric) NSs, elude the detection and we only have upper limits on their intrinsic asymmetry (Aasi et al. 2016), Abbott et al. (2017), and Abbott et al. (2019a), Steltner et al. (2020), Dergachev & Papa (2020)). The community actively pursues many novel methods of detection (see Jaranowski et al. 1998; Krishnan et al. 2004; Antonucci et al. 2008; Astone et al. 2014; Miller et al. 2018; Abbott et al. 2009; Astone et al. 2010; Piccinni et al. 2018; Dupuis & Woan 2005; Dreissigacker et al. 2018; Caride et al. 2019; Dergachev & Papa 2019; Dreissigacker & Prix 2020). Proposed continuous GW emission models include the r-modes (Lindblom et al. 1998; Bildsten 1998; Owen et al. 1998; Andersson et al. 1999) and a fixed rotating axis-asymmetric anisotropy of the quadrupole moment of inertia (Zimmermann & Szedenits 1979; Bonazzola & Gourgoulhon

1996). In this work, we concentrate only on the latter case. For more in-depth review of the current state of GW emission models from NSs, see Andersson et al. (2011); Lasky (2015); Riles (2017); Sieniawska & Bejger (2019).

1.1. Aim of the research

A general estimate of the detectability of a population of NSs in the gravitational emission regime was previously investigated by Regimbau & de Freitas Pacheco (2000), Palomba (2005), Knispel & Allen (2008), and Woan et al. (2018). We revisit this problem by providing a realistic approach to the properties of the estimated population of isolated (solitary, not in a binary system) NSs in our Galaxy, and by more detailed treatment of the detection of the signal. We limit ourselves to a phenomenological parametrization of the deformation of a NS, to find the general constraints on models without investigating physical details that drive the asymmetry of a star. We aim to estimate the fraction of the Galactic population of NSs that can be detected by the Advanced LIGO (Aasi et al. 2015), the Advanced Virgo (Acerese et al. 2015), and by the Einstein Telescope (Punturo et al. 2010; Maggiore et al. 2020). We assume a coherent signal integration time to be $t_{\text{obs}} = 1$ year. Although such period of time is comparable to the current O3 observation run of the LIGO-Virgo collaboration, it should be noted that the usable, scientific data does not cover the whole period (due to maintenance, quality assurance, etc.). Thus, such an estimate is the optimistic upper limit of the possible detection rate.

* mcie@camk.edu.pl

** tb@astrouw.edu.pl

¹ <https://gracedb.ligo.org/superevents/public/O3/>

2. The physical model

As a basis for our studies we use the numerical models developed in our previous work (Cieřlar et al. 2020). We simulated a population of 10^7 isolated NSs², with properties similar to the observed, single radio pulsars in the Galaxy (Manchester et al. 2005)³. In our population synthesis model, we include the evolution of period, period derivative, as well as magnetic field of each NS and trace its position as it moves in the Galactic potential. The magnetic field decay influences the evolution of rotation period and period derivative assuming the magnetic dipole model. We propagate the stars through the Galactic potential, from their birth places (inside the spiral arms), with inclusion of supernova kicks (Hobbs et al. 2005), to their final positions at the current date, when they are observed.

2.1. Kinematics

In our NS model we simulate the initial position distribution of newly born NSs in spiral arms of the Galaxy and we propagate the stars through the Galactic gravitational potential. Since each NS is born during a supernova explosion, we draw the *initial velocity* from the Hobbs et al. (2005) model.

2.2. Period and magnetic field evolution

2.3. Radio luminosity

In our model we simulate two phenomenological radio luminosity models. One is proportional to the *rotational* energy of the NS:

$$L_{\text{rot}} \sim \left(\dot{P}_{15}^{\frac{1}{3}} P^{-1} \right)^{\kappa_1} \quad (1)$$

And the other is a *power-law*

$$L_{\text{p-1}} \sim P^{\kappa_2} \dot{P}_{15}^{\kappa_3} \quad (2)$$

where κ_i are the parameters of the models⁴, and \dot{P}_{15} is a period derivative divided by 10^{-15} . Since both models produce a population that is identical to the observed one, choosing one over another does not have any implication on the evolution of NS in the context of this work. Therefore we use the parameters from the *rotational* model as it contains less parameters.

2.3.1. The age and size of the simulated population

The maximum age of a simulated NS is $t_{\text{age,max}} = 50$ Myr, while the number of stars equals to $N_{\text{pop}} = 10^7$. With an assumption that NS is born every 100 yr, this equals to 20 times higher synthetic population in the last 50 Myr period. The factor 20 was picked due to the technical aspects of the simulation – providing significant sample to compute statistics whereas limiting the simulation time.

The exclusion of NSs older than 50 Myr is dictated by the fact that due to the exponential magnetic decay, implemented in the model, the NSs evolve faster in the period-period derivative plane. While considering their *characteristic age* $\tau = P/2\dot{P}$,

² 10^7 NSs is roughly 20 times more than an expected Galactical population. This number represent a trade-off between statistical error, and computational speed.

³ <http://www.atnf.csiro.au/research/pulsar/psrcat/>

⁴ Symbols describing parameters of the luminosity models where simplified in regards to our previous work (Cieřlar et al. 2020)

Parameter	Value
$\log(\Delta/\text{Myr})$	0.63
$\log(\widehat{B}_{\text{init}}/\text{G})$	12.67
$\log(\sigma_{B_{\text{init}}}/\text{G})$	0.34
$\widehat{P}_{\text{init}}$ s	0.05
$\sigma_{P_{\text{init}}}$ s	0.07

Table 1: The values of the parameters describing the NS evolution model: Δ is the magnetic field decay timescale, $\widehat{B}_{\text{init}}$ and $\sigma_{B_{\text{init}}}$ are the mean initial magnetic field and its dispersion (log-normal distribution), and $\widehat{P}_{\text{init}}$ and $\sigma_{P_{\text{init}}}$ are the mean initial rotation period and its dispersion (positive only, normal distribution).

our population is comparable to the observed one and reaches to characteristic ages of 10 Gyr. Moreover, due to the fact, that older, solitary NS reach a region of period-period derivative plane known as the *graveyard* (a region of periods longer than 1 s) and stay there due to the very low period derivative ($\dot{P} < 10^{-22}$ [s/s]). This region is outside of the frequency range of the current detectors (Advanced LIGO and Advanced Virgo) as well as planned, next generation observatories (Einstein Telescope).

2.3.2. Model parameters

The parameters of the model used in this paper are shown in Table 1. The distributions describing the population’s parameters and details of the pulsar evolution model are described in Cieřlar et al. (2020). The pulsar population model provides us with a population of NSs, and for each of them we have its position in the sky, distance, rotation period, period derivative, and the pulsar age.

2.4. Millisecond Pulsars exclusion from the Model

A standard model for of evolution of Millisecond Pulsars (MSPs) indicate that they are produced due to the accretion in a Low Mass X-ray Binaries (see Bhattacharya & van den Heuvel 1991), although, it should be noted that not all observed MSPs can be confidently described with such model (Kiziltan & Thorsett 2009). Modelling a standard MSP model with an accretion phase requires a very detailed treatment of the binary interactions (e.g. Belczynski et al. 2008). This treatment of binary interactions is beyond scope of our NS evolution model presented in out previous work (Cieřlar et al. 2020), thus we limit this work to the probing of only solitary NSs.

2.5. Gravitational wave signal from a rotating ellipsoid

The GW’s signal registered in the detector is given by the dimensionless amplitude:

$$h = F_+ h_+ + F_\times h_\times. \quad (3)$$

where the F_+ and F_\times (described in detail in Sec. 2.5.2) denote the antenna pattern functions. Since the two wave’s polarisations (+ and \times) are orthogonal, the measured quantity is the root of the square of the h :

$$\sqrt{h^2} = \sqrt{(F_+ h_+ + F_\times h_\times)^2}. \quad (4)$$

We assume a general model of a rotating triaxial ellipsoid after Bonazzola & Gourgoulhon (1996). We do not assume the

cause of the deformation, but merely state that it is necessary for the time-varying quadruple moment of the NS mass (for different theoretical models of NS deformation see Ostriker & Gunn (1969), Melosh (1969), Chau (1970), and Press & Thorne (1972)). The NS's ellipticity is defined as:

$$\epsilon = \frac{|I_1 - I_2|}{I}, \quad (5)$$

where I is the mean NS moment of inertia with respect to the rotational axis, and I_1 and I_2 are moments in the plane perpendicular to the principal axis. The GW's amplitudes in both polarisations can be written as:

$$\begin{aligned} h_+ &= h_0 \sin \chi \left(A \cos \left(\frac{2\pi(t-t_0)}{P} \right) - B \cos \left(\frac{2\pi(t-t_0)}{P/2} \right) \right), \\ h_\times &= h_0 \sin \chi \left(C \sin \left(\frac{2\pi(t-t_0)}{P} \right) - D \sin \left(\frac{2\pi(t-t_0)}{P/2} \right) \right), \end{aligned} \quad (6)$$

where $A = \frac{1}{2} \cos \chi \sin \iota \cos \iota$, $B = \sin \chi \frac{1+\cos^2 \iota}{2}$, $C = \frac{1}{2} \cos \chi \sin \iota$, and $D = \sin \chi \cos \iota$. The NS signal is parametrised by: the angle between the rotation axis and the major axis of the ellipticity χ , the line of sight inclination ι , the rotational period P , the time t , and the time corresponding to a phase-shift t_0 . The amplitude h_0 is defined as:

$$h_0 = \frac{16\pi^2 G}{c^4} \frac{I \epsilon}{P^2 r}, \quad (7)$$

where G is the gravitational constant, c is the speed of light, r distance to the star.

2.5.1. The average emission over the NS Period

Due to parameters A , B , C , and D being independent of the time, we compute an average of h^2 over the period $P = 1/\nu$, where ν is the frequency:

$$\begin{aligned} \langle h^2 \rangle_P &= \langle (F_+ h_+ + F_\times h_\times)^2 \rangle = \\ &= h_0^2 \sin^2 \chi \langle (F_+ A \cos 2\pi\nu t + F_+ B \cos 2\pi 2\nu t \\ &\quad + F_\times C \sin 2\pi\nu t + F_\times D \sin 2\pi 2\nu t)^2 \rangle = \\ &= \frac{1}{2} h_0^2 \sin^2 \chi (F_+^2 (A^2 + B^2) + F_\times^2 (C^2 + D^2)). \end{aligned} \quad (8)$$

The term $\langle h^2 \rangle_P$ represents the average power of emitted GW signal at two harmonics: $\nu = \frac{1}{P}$ and $2\nu = \frac{2}{P}$. In our analysis we emulate the simplest approach of detecting a NS at a single frequency with its amplitude above a certain level (see Seq. 2.6). Therefore, we treat the amplitude of the GW in each frequency independently:

$$\begin{aligned} \langle h^2 \rangle_{P,\nu} &= \frac{1}{2} h_0^2 \sin^2 \chi (F_+^2 A^2 + F_\times^2 C^2), \\ \langle h^2 \rangle_{P,2\nu} &= \frac{1}{2} h_0^2 \sin^2 \chi (F_+^2 B^2 + F_\times^2 D^2). \end{aligned} \quad (9)$$

2.5.2. The antenna pattern and the sidereal day average

The detectors are described by four parameters. Their geographical position longitude and latitude, the angle between their arms, and the angle measured counter-clockwise between the East and the bisector of the arms. The NS location in the sky is described by the equatorial coordinates: the right ascension and the declination, as well as the polarisation angle (the orientation of the

rotation axis with respect to the line of sight). We follow the work of Jaranowski et al. (1998, see Eqs. 10-13 therein) with the antenna power in + and \times wave's polarisations. We average the antenna pattern over one full rotation of the Earth, yielding a final average (over the NS period and a sidereal day). The square of registered GW amplitude is:

$$\langle h^2 \rangle_{P,D} = \frac{1}{2} h_0^2 \sin^2 \chi (\langle F_+^2 \rangle (A^2 + B^2) + \langle F_\times^2 \rangle (C^2 + D^2)). \quad (10)$$

Similar to the Eq. 9, we divide the period-, day-average into two separate harmonics:

$$\begin{aligned} \langle h^2 \rangle_{P,D,\nu} &= \frac{1}{2} h_0^2 \sin^2 \chi (\langle F_+^2 \rangle A^2 + \langle F_\times^2 \rangle C^2), \\ \langle h^2 \rangle_{P,D,2\nu} &= \frac{1}{2} h_0^2 \sin^2 \chi (\langle F_+^2 \rangle B^2 + \langle F_\times^2 \rangle D^2). \end{aligned} \quad (11)$$

2.6. The detectors sensitivity and the signal integration

For the Advanced LIGO and Advanced Virgo detectors, we assume the amplitude spectral density of the noise $\sqrt{S_h(\nu)}$ (expressed in units of strain/ $\sqrt{\text{Hz}}$) from the first three-months of the O3 observation run⁵ to be representative and constant for the whole period of our analysis (Abbott et al. 2018a, living review, see arXiv version for the latest update). We also analyse the future Einstein Telescope (ET-D) in the D configuration (three detection arm pairs in a shape of the equilateral triangle, see Hild et al. (2011)). The location of this facility has not been chosen yet. In that regard, we assume the same location for ET-D as for the Advanced Virgo detector. We scale the sensitivity⁶ appropriately for the D configuration by a factor $1/(\sqrt{3} \sin(\pi/3))$ (see Hild et al. 2011). Also, we sum the signal from its three arms (E1, E2, E3) as $\langle h^2 \rangle_{P,D}^{\text{ET-D}} = \langle h^2 \rangle_{P,D}^{\text{E1}} + \langle h^2 \rangle_{P,D}^{\text{E2}} + \langle h^2 \rangle_{P,D}^{\text{E3}}$.

Since the signal from a NS comes at two harmonics (ν and 2ν , see Eq. 9), we define the signal-to-noise (SNR) ratio (see Jaranowski & Krolak 2009, ch. 7) separately for each harmonic:

$$\text{SNR}_\nu = \frac{\sqrt{\langle h^2_{P,D,\nu} \rangle} \sqrt{t_{\text{obs}}}}{\sqrt{S_h(\nu)}}, \quad \text{SNR}_{2\nu} = \frac{\sqrt{\langle h^2_{P,D,2\nu} \rangle} \sqrt{t_{\text{obs}}}}{\sqrt{S_h(2\nu)}}, \quad (12)$$

where t_{obs} is the integration time. The t_{obs} is far greater than period P or a sidereal day D over which the signal from NS is averaged (see Eq. 11). We assume a detection threshold for a pulsar of $\text{SNR}_{\nu,2\nu} = 11.4$, and the integration time is one year $t_{\text{obs}} = 31536000$ seconds. Thus we use the detectability threshold

$$h_{0,\nu}^* \sim 11.4 \sqrt{\frac{S_h(\nu)}{t_{\text{obs}}}}, \quad h_{0,2\nu}^* \sim 11.4 \sqrt{\frac{S_h(2\nu)}{t_{\text{obs}}}}, \quad (13)$$

and state that a NS is detected in a given harmonic (either ν or 2ν) is the averaged, detected strain crosses the threshold:

$$\sqrt{\langle h^2_{P,D,\nu} \rangle} \geq h_{0,\nu}^*, \quad \sqrt{\langle h^2_{P,D,2\nu} \rangle} \geq h_{0,2\nu}^*. \quad (14)$$

The value for the SNR threshold used in other searches varies from 5 to almost 12. For the O2 blind search (Abbott

⁵ For the sensitivity curves see <https://dcc.ligo.org/LIGO-T2000012/public>.

⁶ For the sensitivity curve see <https://tds.virgo-gw.eu/?content=3&r=14065>.

et al. 2019a) it's equal to 5.3. For both low and high frequency bands in O1 blind search (Abbott et al. 2018c, 2017) the value is equal to 5. In transient signal searches (Abbott et al. 2018b) as well in the narrow-band searches (Abbott et al. 2019b) the SNR/threshold is equal to 8. For the single a single-template search for the known pulsars it's equal to 11.4 after Dreissigacker et al. (2018):

$$h_0^* \sim 11.4 \sqrt{\frac{S_h}{T_{\text{obs}}}} \quad (15)$$

We justify using the value of 11.4 due to the fact that it is most conservative as well as our simulation resembles a single-template search of a known pulsar – we assume that we know the position in the sky and neglect the error associated with it, as well as we compare the signal with a corresponding frequency bin in the detector noise.

2.7. Neutron star asymmetry model

Neutron star must be asymmetric with respect to the rotation axis to emit GWs. There is a plethora of models that predict some level of asymmetry. In this work we do not want to concentrate on any particular physical model. Rather than that we propose a simple, two parameter, phenomenological model of evolution of a NS asymmetry. We assume that there is an initial asymmetry ϵ_0 at the time the NS is formed and it decays on a timescale of η . Thus, at a given moment of time the asymmetry is given by:

$$\epsilon = \epsilon_0 \exp\left(\frac{-t}{\eta}\right). \quad (16)$$

With such a model we can explore a general parameter space of possible mechanisms of asymmetry generation and place observational constraints in such space.

3. Results and discussion

We can now proceed to the estimation of the detectability of the GW form NSs. We use the standard model of properties of NS population (Cieřlar et al. 2020) and for each NS we calculate the expected GW signal-to-noise ratio given its actual position in the sky, distance, period and ellipticity. For each model of evolution of ellipticity characterized by two parameters ϵ_0 and η we calculate the expected number of observed NSs. We normalize our results to a population where a NS is formed in the Milky Way every 100 years, however we estimate the population for a much larger model population (10M stars, 1 every 5yr). Thus, after normalization we can obtain the expected number of observed NSs below unity.

We present the results for the Advanced LIGO Livingston in Figs. 1a and 1b and for the Advanced Virgo detector in Figs. 2a and 2b for the signals' ν and 2ν harmonics respectively (see Eq. 9). The color in these Figs. corresponds to the number of detectable NSs in the entire sky for each model as a function of the parameters ϵ_0 and η . The dark dashed line in each plot corresponds to the models with the expected one detection, and we expect less than one detection in the region of parameter space below this line. A very low number of stars crossing the detection criteria in some regions of the plots may induce arbitrary shapes due to a too low static (most prominently seen on in Figs. 2d and 2c). We disregard such shapes as a significant increase of simulated stars would be needed to smooth the low-detection region in Figs. 1 and 2. The detectability of pulsar population with

harmonic	SNR	V1	L1	H1	ET
ν	11.4	0	0.05	0.05	2.3
2ν	11.4	0	0.1	0.15	26.4
ν	5	0	0.1	0.05	7.15
2ν	5	0.1	0.7	0.5	82.0

Table 2: The expected number of detection for a model with parameters equal to: $\epsilon_0 = 10^{-5}$ and $\eta = 10^4$ Myr. The numbers are normalised to an estimated number of Galactic NSs.

Advanced detectors with the noise level factor two lower (below 200Hz) then the current one, could improve the detectability by factor of 3 for the H1 detector and factor 7 for the L1 detector. Though, such increase would remain below a single detected NS.

For the models where the population evolves slowly, i.e. $\eta > 0.1$ Myr, we expect at least one detection, for the 2ν harmonic, with the Advanced LIGO detectors provided that the initial ellipticity $\epsilon_0 > 2.5 \times 10^{-5}$ and $\epsilon_0 > 6.3 \times 10^{-5}$ for the Advanced Virgo detector. For the population of quickly evolving ellipticity the detectability quickly becomes more and more difficult as the timescale η decreases. This is due to the fact the number of NSs with sufficiently large ellipticity in the Milky Way at a given time becomes smaller and smaller.

The similar diagrams calculated for the sensitivity of ET are shown in Figs. 2c and 2d. For this detector in the regime of slowly varying ellipticity, i.e. with $\eta > 0.1$ Myr the detectable models have the initial ellipticity $\epsilon_0 > 7.9 \times 10^{-7}$ for the 2ν harmonic, and $\epsilon_0 > 5.6 \times 10^{-6}$ for the ν harmonic. The population becomes undetectable for $\eta < 100$ yr, as in this case the ellipticity decreases on the timescale comparable to the time between consecutive supernovae explosions in the Galaxy.

It is quite interesting to investigate in more detail the properties of the detectable population. In Fig. 3 we present the maximum age of pulsars in the detectable population as a function of the model parameters η and ϵ_0 for the case of Advanced Virgo and the Einstein Telescope. For detectable NSs in all models, for the current Advanced detectors, the maximum age is not larger than 1 Myr – this is due to the fact that only the youngest NSs crossed the threshold of the detection.

Let us now concentrate on a single model with a 2.3 and 26.4 detections, for the ν and 2ν harmonics respectively, in the Einstein Telescope described by $\epsilon_0 = 10^{-5}$ and $\eta = 10^4$ Myr (see Tab. 2). In Figs. 4 and 5, we present the population of NSs on a diagram spanned by the GW frequency and the mean value of the GW amplitude. We also plot the detection threshold curves corresponding to one year integration and SNR threshold 11.4 for the current detectors and for ET-D. We note that the detectable populations will change by a factors ranging from 3 for the H1 detector to 7 for the L1 detector if the threshold is lowered to SNR = 5. In comparison, ET-D will increase its number of visible NSs only by a factor of 3. The discrepancy is due to the very poor statistics of the easiest to detect NSs, which leads to conclusion that a factor equal to 7 may be an overestimate.

The density of the population of NSs is shown as a color map. The observable NSs have frequencies in the range of approximately 10 to 300 Hz, with rare NSs going above 300 Hz, when searching for the signal's 2ν harmonic (see Fig. 6), and correspondingly lower for the signal's ν harmonic. In Fig. 7 we compare the detectable, GW population (the color represents the amplitude of the signal's 2ν harmonic) with the population of single pulsars in the Galaxy (based on the Australia Telescope National Facility Pulsar Catalogue's, Manchester et al. (2005)). The population of NSs that can be detected in ET-D resides mostly in the

upper left corner of the period – period derivative plane, which corresponds to the very young NSs. Since NSs are born in the Galactic disk, this leads to a spatially concentrated distribution (see Fig. 8).

In Figure 6 we present the population of pulsars detectable in ET in the space of variables used in gravitational wave searches: frequency and frequency derivative. The typical values of the frequency derivative $\dot{\nu}$ are in the range from 10^{-18} Hz^2 to 10^{-8} Hz^2 . Thus most of the potentially detectable pulsars have frequency derivative that is not detectable. The frequencies of the detectable pulsars all lie below 300 Hz, and the bulk of the detectable objects have frequencies in the range from 10 Hz to 60 Hz.

As a result, the optimal strategy to look for GW from isolated rotating NSs concentrate the surveys on the Galactic disk. In the case of the Advanced detectors we expect detected pulsars only at 2ν harmonic with frequencies in the range of 30–300 Hz. In the case of the ET the bulk of detections will be in the frequency range from 20 to 100 Hz for the ν harmonic and 10 to 100 Hz for the 2ν harmonic. The frequency derivatives of the brightest systems are above 10^{-8} Hz^2 , while the typical values will be of frequency derivative in the population detectable by the ET is from 10^{-12} to 10^{-9} Hz^2 . The largest value of the frequency derivative in the recent search Abbott et al. (2019a) was only 10^{-8} Hz^2 . Narrowing down the parameter space for the searches as suggested above will increase the chances of detection.

3.1. Limitation of the model – Millisecond Pulsars

If we inspect all detected pulsars (see green and blue populations on Fig. 7) we note that the MSPs (green population) reside mostly in the frequency range from 200 Hz to 2 kHz for the more prominent harmonic of $f_{\text{GW}} = 2f_{\text{NS}}$. Their addition could improve the detection prospects. However, answering question about quantitative improvement would require addressing the binary interactions (mentioned in 2.4 as well as more detailed model of asymmetry model that treats the initial and accretion induced inhomogeneity of the NS momentum).

4. Conclusions

We presented our estimation of the detectability of the Galactic population of isolated NSs. With a high value of the initial ellipticity ($\epsilon_0 \approx 10^{-5}$) and no decay in the moment of inertia non-uniformity (decay scale $\eta = t_{\text{hub}} \approx 10^4 \text{ Myr}$), the expected number of detected NSs in the Advanced Detectors is still less than 1. Since the increase in signal-to-noise is proportional to square root of time (signal-to-noise $\sim \sqrt{t_{\text{obs}}}$), we do not expect a drastic change in the estimates for the Advanced LIGO and Advanced Virgo detectors. The most limiting factor is the low frequency sensitivity (below 100 Hz) of the detectors. As shown in Fig. 2c, we expect that future experiments such as the Einstein Telescope will clearly improve the prospect of continuous GW signal discovery.

We present the parameter space of the most likely discovery of solitary pulsars: the range frequencies, frequency derivatives and position in the sky. We suggest that narrowing down searches in this restricted parameter space may increase effective sensitivity and increase a chance of detection.

Acknowledgements. We would like to thank Brynmore Haskell and Graham Woan for comments and fruitful discussion. MC and TB are supported by the grant ‘‘AstroCeNT: Particle Astrophysics Science and Technology Centre’’ (MAB/2018/7) carried out within the International Research Agendas pro-

gramme of the Foundation for Polish Science (FNP) financed by the European Union under the European Regional Development Fund. Part of this work was supported by Polish National Science Centre (NCN) grants no. 2016/22/E/ST9/00037 and 2017/26/M/ST9/00978. TB, MS, and NS acknowledge support of the TEAM/2016-3/19 grant from FNP. MS was partially supported by the NCN grant no. 2018/28/T/ST9/00458.

References

- Aasi, J., Abbott, B. P., Abbott, R., et al. 2015, *Classical and Quantum Gravity*, 32, 074001
- Aasi, J., Abbott, B. P., Abbott, R., et al. 2016, *Phys. Rev. D*, 93, 042007
- Abbott, B., Abbott, R., Adhikari, R., et al. 2009, *Physical Review D - Particles, Fields, Gravitation and Cosmology*, 79
- Abbott, B. P., Abbott, R., Abbott, T. D., et al. 2018a, *Living Reviews in Relativity*, 21, 3
- Abbott, B. P., Abbott, R., Abbott, T. D., et al. 2018b, *Classical and Quantum Gravity*, 35, 065009
- Abbott, B. P., Abbott, R., Abbott, T. D., et al. 2016, *Phys. Rev. Lett.*, 116, 061102
- Abbott, B. P., Abbott, R., Abbott, T. D., et al. 2019, *Phys. Rev. X*, 9, 031040
- Abbott, B. P., Abbott, R., Abbott, T. D., et al. 2019a, *Phys. Rev. D*, 100, 024004
- Abbott, B. P., Abbott, R., Abbott, T. D., et al. 2019b, *Phys. Rev. D*, 99, 122002
- Abbott, B. P., Abbott, R., Abbott, T. D., et al. 2017, *Phys. Rev. Lett.*, 119, 161101
- Abbott, B. P., Abbott, R., Abbott, T. D., et al. 2018c, *Phys. Rev. D*, 97, 102003
- Abbott, B. P., Abbott, R., Abbott, T. D., et al. 2017, *Phys. Rev. D*, 96, 062002
- Abbott, B. P., Abbott, R., Abbott, T. D., et al. 2017, *Phys. Rev. D*, 96, 122004
- Abbott, B. P., Abbott, R., Abbott, T. D., et al. 2017, *ApJ*, 848, L12
- Abbott, R., Abbott, T. D., Abraham, S., et al. 2020, *arXiv e-prints*, arXiv:2010.14527
- Acernese, F., Agathos, M., Agatsuma, K., et al. 2015, *Classical and Quantum Gravity*, 32, 024001
- Andersson, N., Ferrari, V., Jones, D. I., et al. 2011, *General Relativity and Gravitation*, 43, 409
- Andersson, N., Kokkotas, K. D., & Stergioulas, N. 1999, *The Astrophysical Journal*, 516, 307
- Antonucci, F., Astone, P., Antonio, S. D., Frasca, S., & Palomba, C. 2008, *Classical and Quantum Gravity*, 25, 184015
- Astone, P., Colla, A., D’Antonio, S., Frasca, S., & Palomba, C. 2014, *Phys. Rev. D*, 90, 042002
- Astone, P., D’Antonio, S., Frasca, S., & Palomba, C. 2010, *Classical and Quantum Gravity*, 27, 194016
- Belczynski, K., Kalogera, V., Rasio, F. A., et al. 2008, *ApJS*, 174, 223
- Bhattacharya, D. & van den Heuvel, E. P. J. 1991, *Phys. Rep.*, 203, 1
- Bildsten, L. 1998, *The Astrophysical Journal*, 501, L89
- Bonazzola, S. & Gourgoulhon, E. 1996, *A&A*, 312, 675
- Caride, S., Inta, R., Owen, B. J., & Rajbhandari, B. 2019, *Phys. Rev. D*, 100, 064013
- Chau, W. Y. 1970, *Nature*, 228, 655
- Cieřlar, M., Bulik, T., & Ostrowski, S. 2020, *MNRAS*, 492, 4043
- Dergachev, V. & Papa, M. A. 2019, *Phys. Rev. Lett.*, 123, 101101
- Dergachev, V. & Papa, M. A. 2020, *Phys. Rev. Lett.*, 125, 171101
- Dreissigacker, C. & Prix, R. 2020, *Phys. Rev. D*, 102, 022005
- Dreissigacker, C., Prix, R., & Wette, K. 2018, *Phys. Rev. D*, 98, 084058
- Dupuis, R. J. & Woan, G. 2005, *Phys. Rev. D*, 72, 102002
- Hild, S., Abernathy, M., Acernese, F., et al. 2011, *Classical and Quantum Gravity*, 28, 094013
- Hobbs, G., Lorimer, D. R., Lyne, A. G., & Kramer, M. 2005, *MNRAS*, 360, 974
- Jaranowski, P. & Krolak, A. 2009, *Analysis of Gravitational-Wave Data*, Cambridge Monographs on Particle Physics, Nuclear Physics and Cosmology No. 29 (Cambridge University Press)
- Jaranowski, P., Królak, A., & Schutz, B. F. 1998, *Phys. Rev. D*, 58, 063001
- Kiziltan, B. & Thorsett, S. E. 2009, *ApJ*, 693, L109
- Knispel, B. & Allen, B. 2008, *Phys. Rev. D*, 78, 044031
- Krishnan, B., Sintes, A. M., Papa, M. A., et al. 2004, *Phys. Rev. D*, 70, 082001
- Lasky, P. D. 2015, *PASA*, 32, e034
- Lindblom, L., Owen, B. J., & Morsink, S. M. 1998, *Phys. Rev. Lett.*, 80, 4843
- Maggiore, M., Broeck, C. V. D., Bartolo, N., et al. 2020, *Journal of Cosmology and Astroparticle Physics*, 2020, 050
- Manchester, R. N., Hobbs, G. B., Teoh, A., & Hobbs, M. 2005, *AJ*, 129, 1993
- Melosh, H. J. 1969, *Nature*, 224, 781
- Miller, A., Astone, P., D’Antonio, S., et al. 2018, *Phys. Rev. D*, 98, 102004
- Ostriker, J. P. & Gunn, J. E. 1969, *ApJ*, 157, 1395
- Owen, B. J., Lindblom, L., Cutler, C., et al. 1998, *Phys. Rev. D*, 58, 084020
- Palomba, C. 2005, *MNRAS*, 359, 1150
- Piccinni, O. J., Astone, P., D’Antonio, S., et al. 2018, *Classical and Quantum Gravity*, 36, 015008
- Press, W. H. & Thorne, K. S. 1972, *ARA&A*, 10, 335

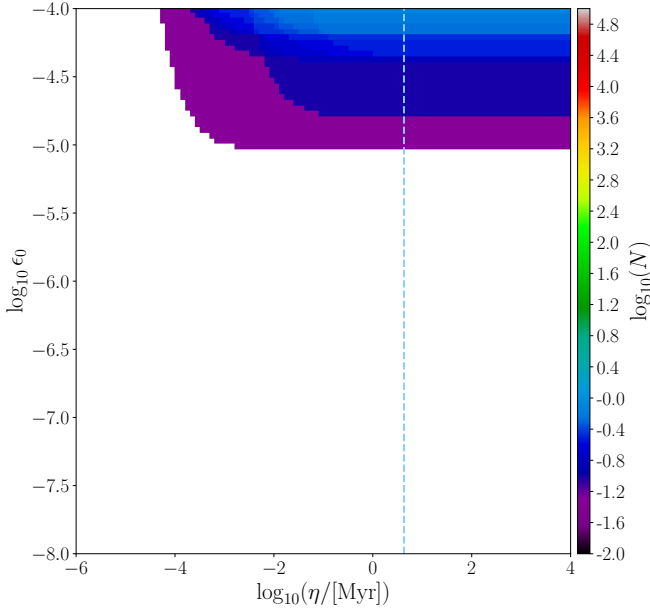
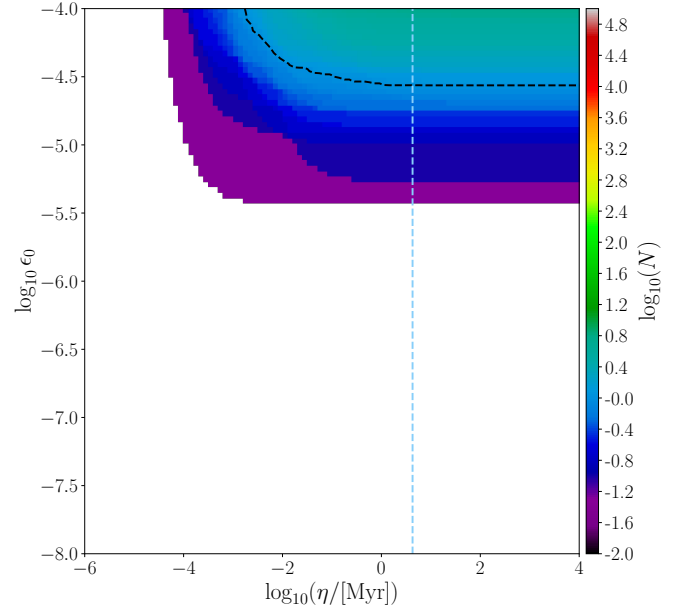
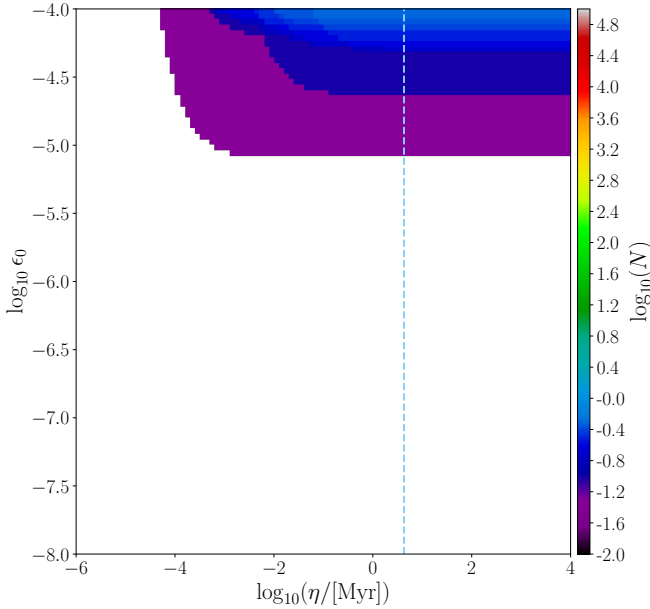
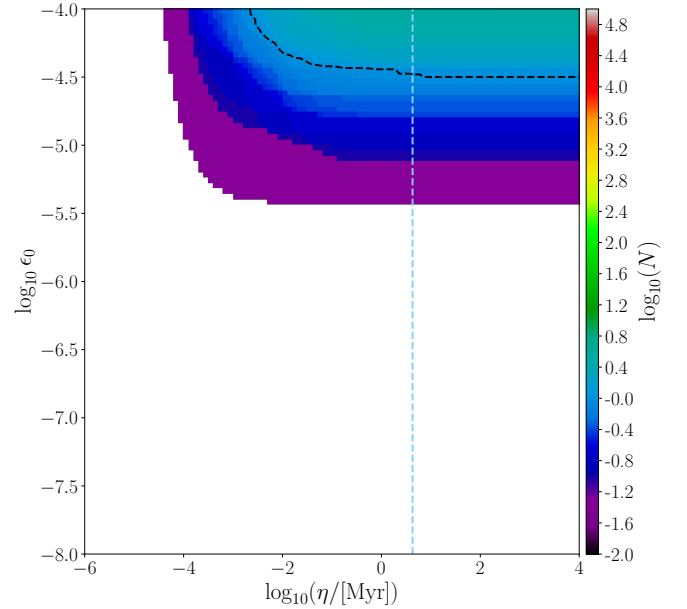

(a) ν . L1 Advanced LIGO detector at Livingston.

(b) 2ν . L1 Advanced LIGO detector at Livingston.

(c) ν . H1 Advanced LIGO detector at Hanford.

(d) 2ν . H1 Advanced LIGO detector at Hanford.

Fig. 1: The number of observable pulsars in one year observations in the space of the parameters of the model $\eta - \epsilon_0$ for the Advanced LIGO detectors. The left column corresponds to the signal's ν harmonic, the right column the 2ν harmonic. The color represents the expected number of detection for each model. The black dashed line in each plot corresponds to the models where we expect to see one pulsar. All models below the black dashed line correspond to less than one expected detection. The blue, vertical, dashed line indicates models where η is equal to the magnetic field decay Δ (see Tab. 1).

Punturo, M., Abernathy, M., Acernese, F., et al. 2010, *Classical and Quantum Gravity*, 27, 194002
Regimbau, T. & de Freitas Pacheco, J. A. 2000, *A&A*, 359, 242
Riles, K. 2017, *Modern Physics Letters A*, 32, 1730035
Rudak, B. & Ritter, H. 1994, *Monthly Notices of the Royal Astronomical Society*, 267, 513
Sieniawska, M. & Bejger, M. 2019, *Universe*, 5, 217
Steltner, B., Papa, M. A., Eggenstein, H. B., et al. 2020, *arXiv e-prints*, arXiv:2009.12260

Woan, G., Pitkin, M. D., Haskell, B., Jones, D. I., & Lasky, P. D. 2018, *The Astrophysical Journal*, 863, L40
Zimmermann, M. & Szedenits, E. 1979, *Phys. Rev. D*, 20, 351

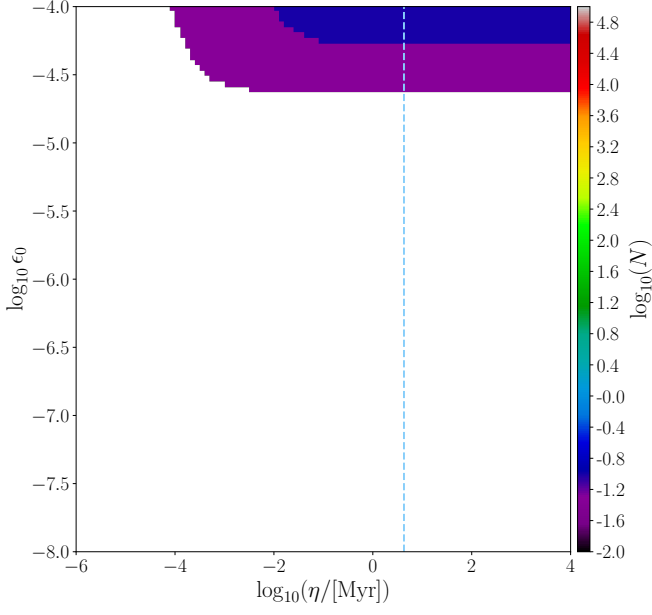
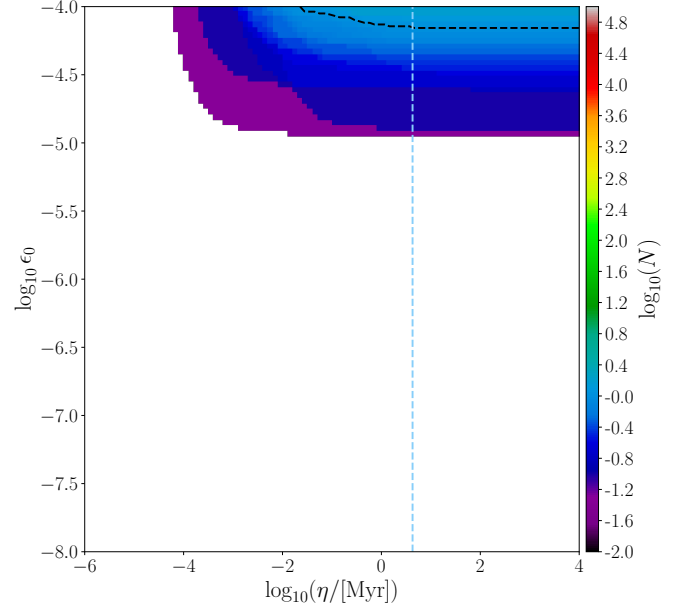
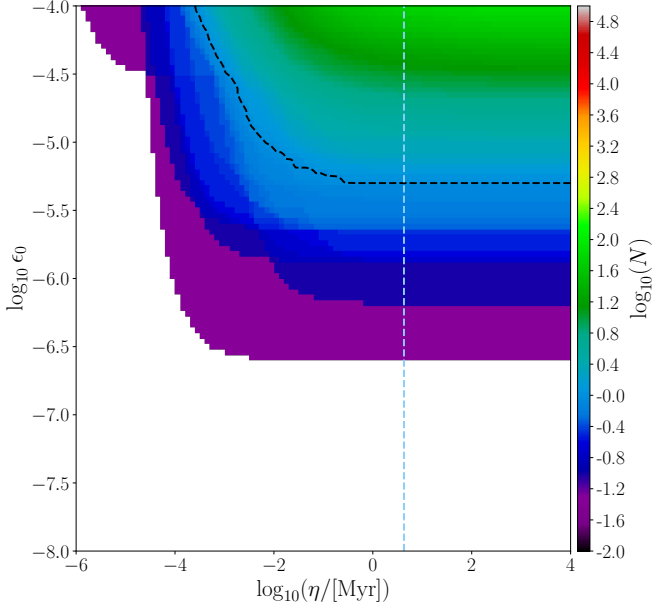
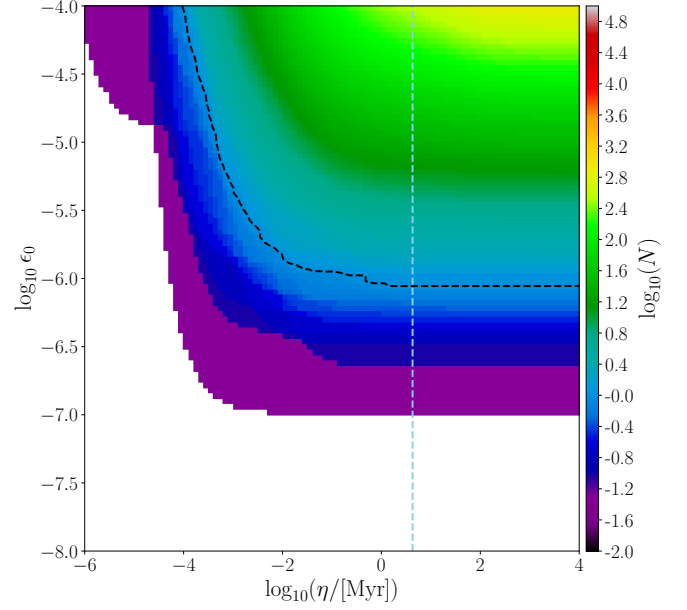

 (a) ν . V1 Advanced Virgo detector.

 (b) 2ν . V1 Advanced Virgo detector.

 (c) ν . ET-D Einstein Telescope detector, configuration D.

 (d) 2ν . ET-D Einstein Telescope detector, configuration D.

Fig. 2: The number of observable pulsars in one year observations in the space of the parameters of the model $\eta - \epsilon_0$ for the Advanced Virgo, and Einstein Telescope detectors. The left column corresponds to the signal's ν harmonic, the right column the 2ν harmonic. The black dashed line in each plot corresponds to the models where we expect to see one pulsar. All models below the black dashed line correspond to less than one expected detection. The blue, vertical, dashed line indicates models where η is equal to the magnetic field decay Δ (see Tab. 1).

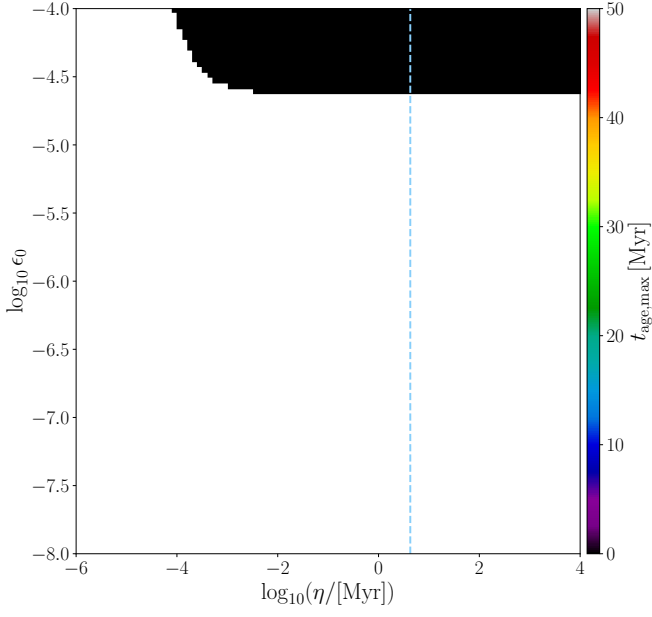
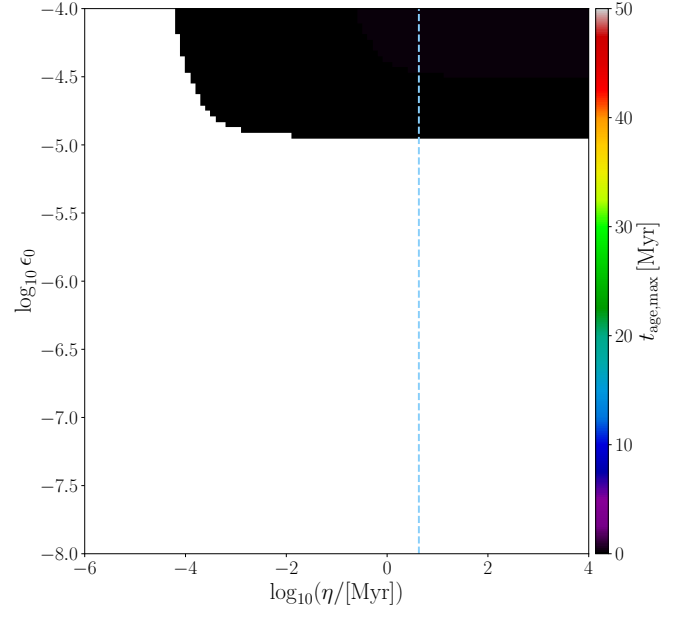
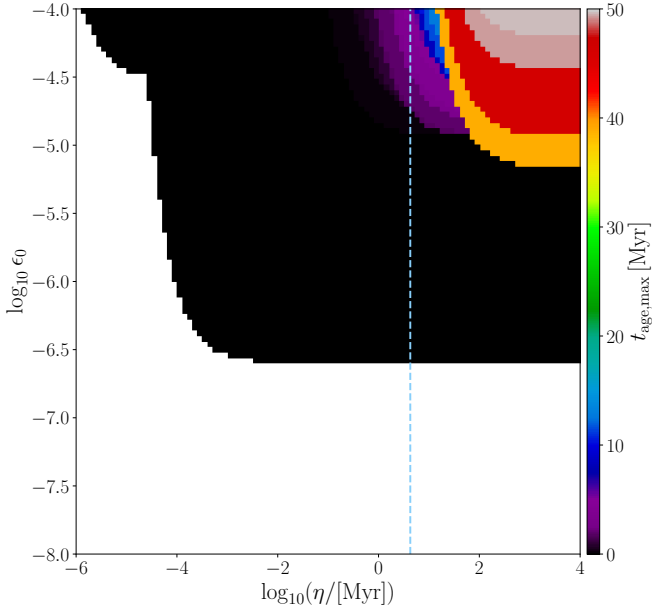
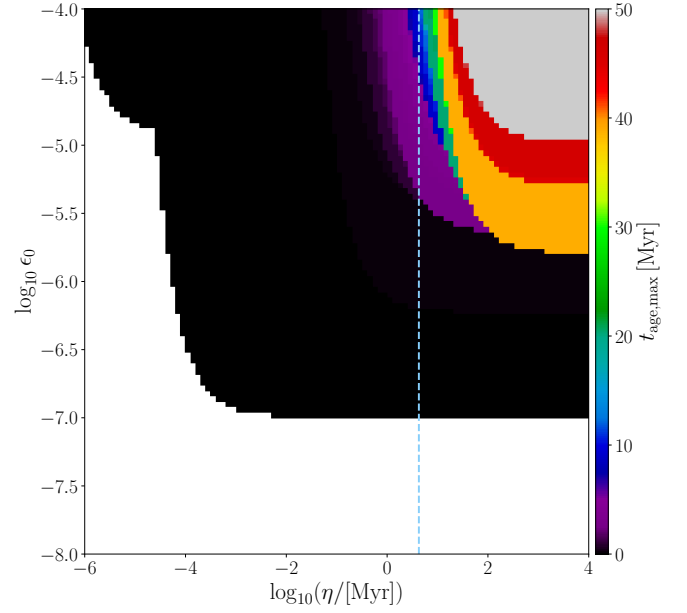

(a) ν . V1 Advanced Virgo detector.

(b) 2ν . V1 Advanced Virgo detector.

(c) ν . Einstein Telescope detector, configuration D.

(d) 2ν . Einstein Telescope detector, configuration D.

Fig. 3: The maximum age of visible NSs in one year observations in the space of the parameters of the model $\eta - \epsilon_0$ for the Advanced Virgo, and Einstein Telescope detectors. The left column corresponds to the signal's ν harmonic, the right column the 2ν harmonic. The color represents the maximum age in the population for a given model. The blue, vertical, dashed line indicates models where η is equal to the magnetic field decay Δ (see Tab. 1).

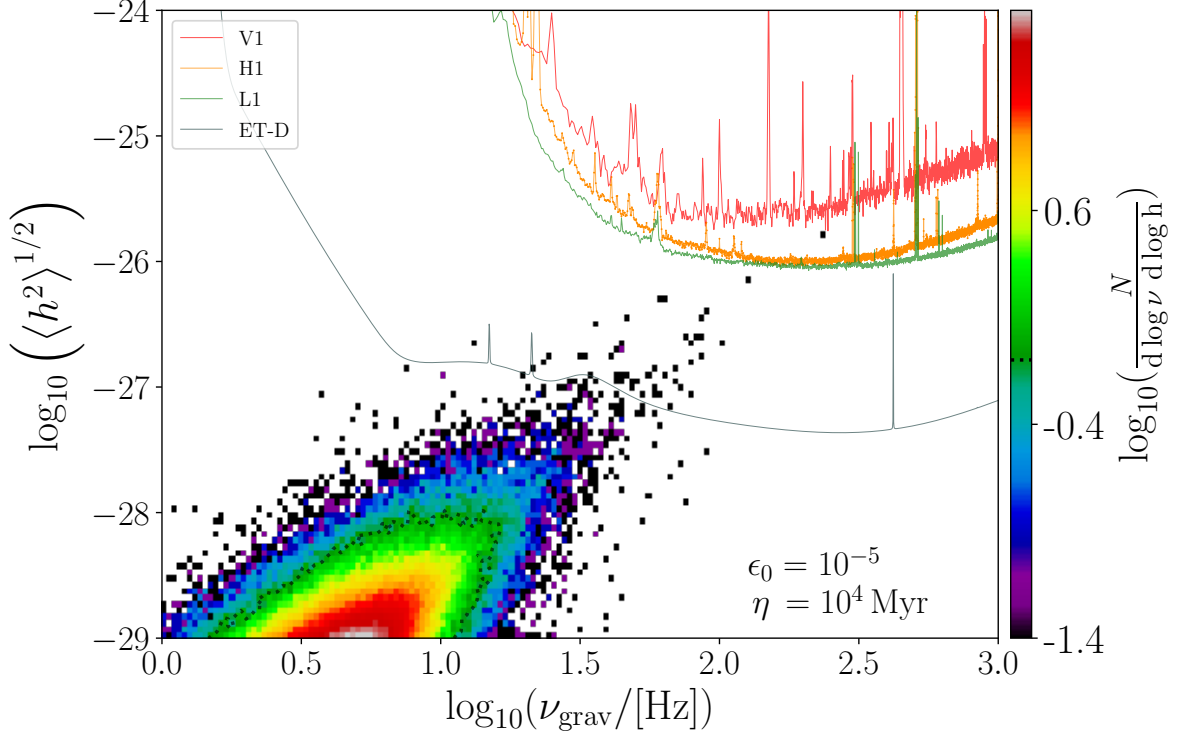


Fig. 4: The sensitivity curves for the Advanced LIGO (L1, H1), the Advanced Virgo (V1), and the Einstein Telescope in configuration D detectors for the signal's ν harmonic of the population of NSs. Model parameters equal to $\epsilon_0 = 10^{-5}$, and $\eta = 10^4$ Myr. The sensitivity of the detectors is scaled by one year of integration time ($\times 1/\sqrt{t_{\text{obs}}}$). The colour represents the density of NS population. The measured h is estimated to for the ET.

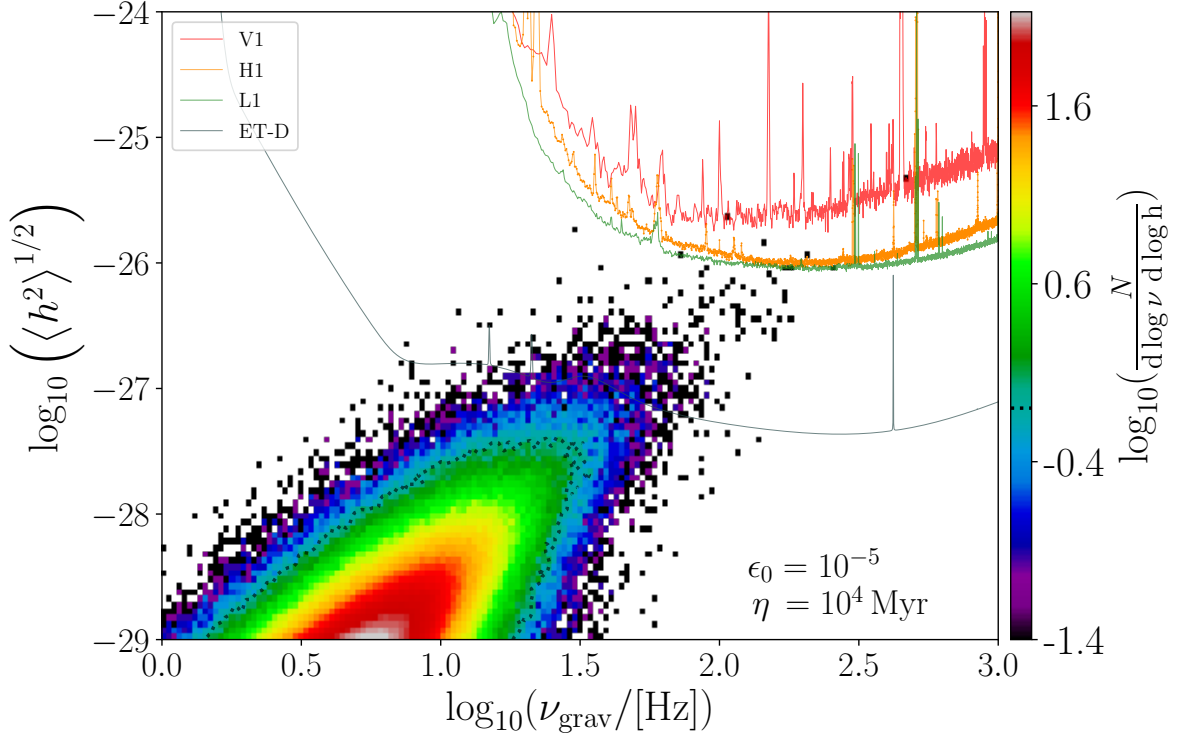


Fig. 5: The sensitivity curves for the Advanced LIGO (L1, H1), the Advanced Virgo (V1), and the Einstein Telescope in configuration D detectors for the signal's 2ν harmonic of the population of NSs. Model parameters equal to $\epsilon_0 = 10^{-5}$, and $\eta = 10^4$ Myr. The sensitivity of the detectors is scaled by one year of integration time ($\times 1/\sqrt{t_{\text{obs}}}$). The colour represents the density of NS population. The measured h is estimated to for the ET.

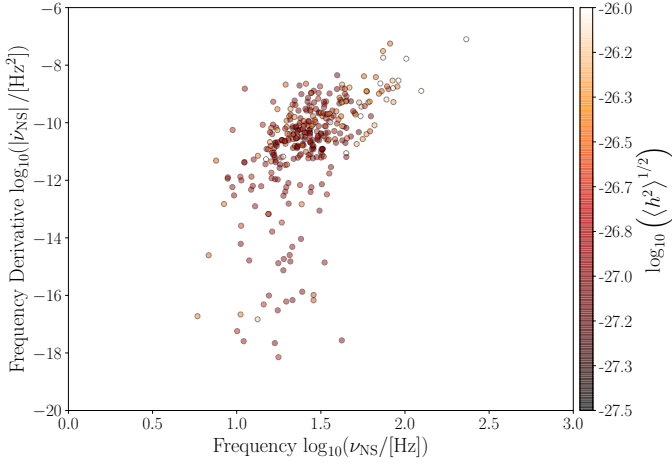


Fig. 6: The frequency – frequency derivative plane. The color represents the emitted GW at 2ν frequency for the Einstein Telescope, configuration D, for one year of integration time. Model parameters equal to $\epsilon_0 = 10^{-5}$, $\eta = 10^4$. The presented population is $\times 20$ larger than the expected Galactic population.

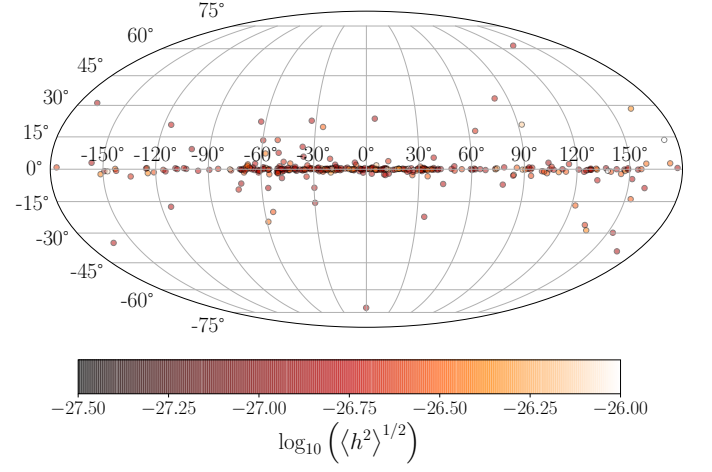


Fig. 8: Spatial distribution in the Galactic coordinates of visible population in the Einstein Telescope configuration D, at the 2ν frequency, model parameters equal to $\epsilon_0 = 10^{-5}$, $\eta = 10^4$.

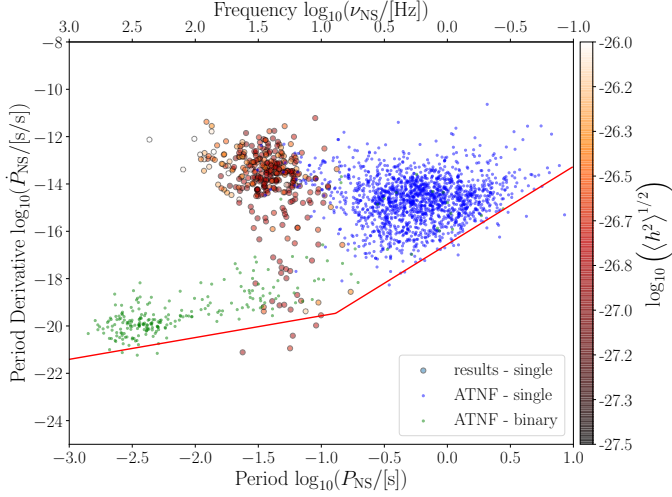


Fig. 7: The period – period derivative plane. The color represents the emitted GW at 2ν frequency for the Einstein Telescope, configuration D, for one year of integration time. Model parameters equal to $\epsilon_0 = 10^{-5}$, $\eta = 10^4$. The presented population is $\times 20$ higher than the expected Galactic population. The blue dots represent the population of observed, single pulsars. The green dots – population of observed pulsars in binary systems (MSPs). Observed populations are from the Australia Telescope National Facility (ATNF) Pulsar Catalogue’s (Manchester et al. 2005). The red lines represent the *death lines* – theoretical limit for an effective radio emission (Rudak & Ritter 1994).